

Isolated-attosecond-pulse generation due to the nuclear dynamics of H_2^+ in a multicycle midinfrared laser field

Yinghui Zheng, Zhinan Zeng,* Ruxin Li,† and Zhizhan Xu

State Key Laboratory of High Field Laser Physics, Shanghai Institute of Optics and Fine Mechanics,
Chinese Academy of Sciences, Shanghai, 201800, China

(Received 6 November 2011; published 17 February 2012)

A scheme is proposed to generate isolated attosecond pulses in the water window driven by a multicycle 2400-nm midinfrared laser field with moderate intensity interacting with H_2^+ molecules. Single attosecond pulses are achieved due to the charge resonance-enhanced ionization and nuclear motion by the numerical solutions of a non-Born-Oppenheimer time-dependent Schrödinger equation. Thus, the single attosecond pulse generation provides insight into the nuclear dynamics.

DOI: [10.1103/PhysRevA.85.023410](https://doi.org/10.1103/PhysRevA.85.023410)

PACS number(s): 32.80.Rm, 42.65.Ky

I. INTRODUCTION

High-order harmonic generation (HHG) induced by the interaction of a high-intensity laser pulse with atoms or molecules is proved to be an effective way to generate an extreme ultraviolet (XUV) source [1,2] and an isolated attosecond pulse [3], which have already proven ideal for capturing the motion of electrons in atoms, molecules, and materials [4,5].

In the so-called water window, from 4.4 to 2.3 nm (from 280 to 550 eV), water is comparatively transparent and organic materials are absorptive for carbon-containing biological samples. Thus, high-contrast biological spectroscopy in this spectral window has long been one of the most important objectives of the development of coherent XUV sources [6]. The generation of isolated attosecond pulses in the water window has an extremely vital significance for studying the ultrafast electronic dynamics of biological samples in water. With the rapid development in ultrafast laser technology, the intense ultrafast laser sources in the midinfrared region have been achieved [7–10] and have been employed experimentally [2,11], which makes it possible to realize the attosecond pulse generation in the water window. Several approaches have so far been proposed to achieve single attosecond pulses in this spectral region, including the detuned midinfrared two-color scheme [12], midinfrared polarization gating modulated by a weaker linearly polarized pulse [13,14], and the double optical gating with very high intensity [15]. However, the above methods have high demands for the driving laser field and depend on a complex shaped laser field. Thus we aim to find an approach to generate isolated attosecond pulses in the water window based on the directly available driving laser pulses with moderate intensity.

Compared to atoms, molecules inevitably introduce a further complexity in harmonic generation due to the additional degree of freedom for nuclear wave packet motion, including charge resonance-enhanced ionization (CREI) at distances larger than equilibrium [16,17], the molecular bond being softened by multiphoton couplings [18]. Molecules in the

strong-field process were investigated earlier at fixed inter-nuclear distance from the Born-Oppenheimer approximation, which ignores the couplings of the electronic and nuclear wave packet. Recently, non-Born-Oppenheimer (NBO) time-dependent Schrödinger equation (TDSE) simulations have revealed a variety of unique nonlinear responses, such as allowing the shortening of the trains of generated attosecond pulses [19] and monitoring electron-nuclear dynamics on an attosecond time scale since the harmonic signal can be modified by the nuclear motion [20,21].

In the present work, we propose a scheme to produce isolated attosecond pulses in the water window using a 2400-nm midinfrared laser pulse with moderate intensity interacting with H_2^+ molecules. By using numerical solutions of NBO TDSE, single attosecond pulses are achieved resulting from the nuclear motion. Thus, the nuclear dynamics could be reflected from the generation of single attosecond pulses.

II. THEORETICAL MODEL

In our work, we follow the numerical treatment described in Ref. [22]. Up to now, the HHG of the aligned molecules has been a proven technique [23–25]. Therefore, the molecular axis is assumed to be parallel to the polarization direction of the linearly polarized laser field and electron moves along the molecular axis. Here the moving electron and nuclei are allowed to be calculated using complete one-dimensional (1D) TDSE. Such a simplified 1D H_2^+ model has been verified by many previous studies [19,23,26,27]. The 1D TDSE is written as ($e = \hbar = m_e = 1$ in atomic units (a.u.), which are used throughout unless otherwise indicated):

$$i \frac{\partial \psi(z, R, t)}{\partial t} = [T_R + T_e + V(z, R) + V_I(z, t)] \psi(z, R, t), \quad (1)$$

where R is the relative nuclear coordinate, and z is the electronic coordinate with respect to the center of mass of the two nuclei. $T_R = -\frac{1}{m_p} \frac{\partial^2}{\partial R^2} + \frac{1}{R}$ and $T_e = -\frac{1}{2\gamma} \frac{\partial^2}{\partial z^2}$ denote the nuclear and electronic kinetic-energy operators, respectively. $m_p = 1836$ is the proton mass, and $\gamma = \frac{2m_p}{1+2m_p}$ is the nuclei-electron reduced mass. The soft-Coulomb potential $V(z, R)$ reads

$$V(z, R) = -\frac{1}{\sqrt{(z + R/2)^2 + 1}} - \frac{1}{\sqrt{(z - R/2)^2 + 1}}. \quad (2)$$

*zhinan_zeng@mail.siom.ac.cn

†ruxinli@mail.shenc.ac.cn

The external interaction $V_I(z, t)$ between the laser field and molecule reads

$$V_I(z, t) = -\frac{2m_p + 2}{2m_p + 1} zE(t), \quad (3)$$

where $E(t) = E_0 f(t) \sin(\omega t)$ denotes the linearly polarized driving field with peak amplitude E_0 , envelope function $f(t)$, and frequency ω . In the TDSE calculations, the Schrödinger equation (1) is numerically solved by the second-order split-operator technique [28]. The high harmonic intensity spectrum is proportional to the squared modulus of the Fourier transform of the dipole acceleration expectation value.

In the simulation, we employ an envelope function $f(t) = \sin(\pi t/T)^2$, where T is the total pulse duration. The ground state of the field-free H_2^+ molecular system with Hamilton operator $H_0 = T_R + T_e + V(z, R)$, obtained by propagating the field-free Schrödinger equation in imaginary time [29], is chosen to be the initial wave function. The H_2^+ molecular ground-state energy is set to be -21.1 eV. The wave function $\psi(z, R, t)$ is discrete on a two-dimensional grid containing 16384 grid points on the z axis with the step of 0.2 a.u. and 1024 grid points in the R axis with the step of 0.05 a.u. The time step of wave function propagation is $dt = 0.08$ a.u. In order to avoid spurious reflections of the wave packet from the boundary, the wave function is multiplied by a $\cos^{1/8}$ mask function [30].

III. RESULTS AND DISCUSSION

The high-order harmonic spectra are shown in Fig. 1 for the H_2^+ molecule (red solid curve) and the H atom (blue dotted curve) respectively, driven by the laser pulse with a peak intensity of 4×10^{14} W/cm², a wavelength of 2400 nm, and a duration (the full width at half maximum) of about four optical cycles shown in the inset of Fig. 1. In the simulation, the softening parameter is properly set for the H atom so that its ground-state energy is equal to that of the H_2^+ molecule $E_0 = -21.1$ eV. As can be seen, the harmonic intensity of the H_2^+ molecule is about one order of magnitude lower than that of the H atom for the spectral region higher than ~ 270 eV.

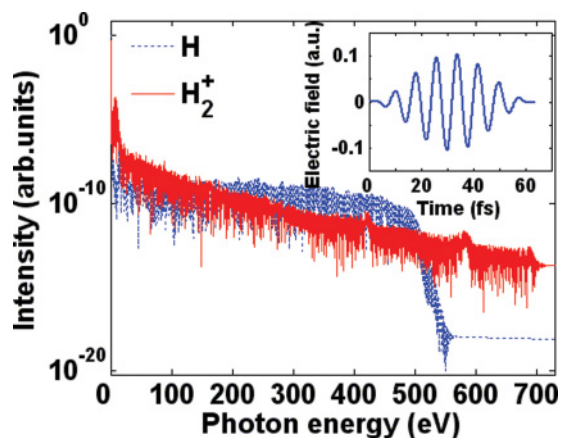


FIG. 1. (Color online) High-order harmonic spectra for the H_2^+ molecule (red solid curve) and the H atom (blue dotted curve), respectively. The inset shows the sketch of the driving laser pulse with a peak intensity of 4×10^{14} W/cm² and a wavelength of 2400 nm.

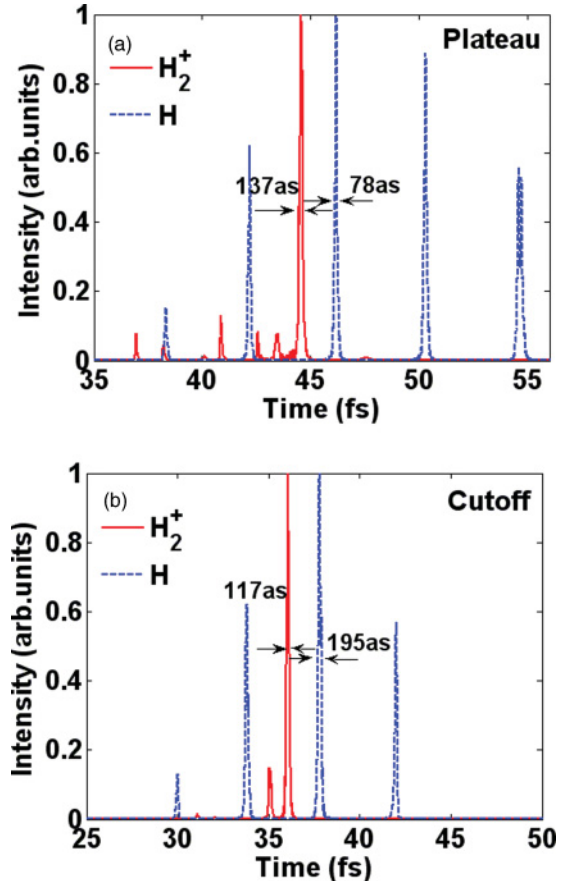


FIG. 2. (Color online) Temporal profiles of the harmonic emission by performing an inverse Fourier transform of the spectra from 258 to 323 eV in the plateau region (a), and in the cutoff (b) (from 626 to 691 eV for the H_2^+ molecule and from 433 to 497 eV for the H atom, respectively).

Nevertheless, the cutoff energy is extended from 497 eV for the H atom to 691 eV for the H_2^+ molecule.

Figure 2 shows the temporal profiles of the harmonic emission by performing an inverse Fourier transform of the spectra from 258 to 323 eV in the plateau region [Fig. 2(a)], and in the cutoff [Fig. 2(b)] from 626 to 691 eV for the H_2^+ molecule as well as from 433 to 497 eV for the H atom, respectively. One can see that an isolated attosecond pulse is generated not only in the cutoff but also in the region of plateau for the H_2^+ molecule taking the nuclear motion into account, while attosecond pulse trains are obtained for the H atom. The durations of the single attosecond pulse generated in the plateau region and in the cutoff are 137 as and 117 as, respectively. In the calculations we scan the position and bandwidth of the spectrum, and the spectrum from 258 to 323 eV in the plateau region and that from 626 to 691 eV in the cutoff are found to be optimal to achieve an isolated attosecond pulse. It also can be seen from these figures that the generated isolated attosecond pulses are accompanied by several weak pulses, which result from the modulation of the spectra shown in Fig. 1 due to the interference between the continuum spectra close to each other. The maximum ratios of weak pulses to the main pulse are 1:8 in the plateau region and 1:7 in the cutoff, respectively.

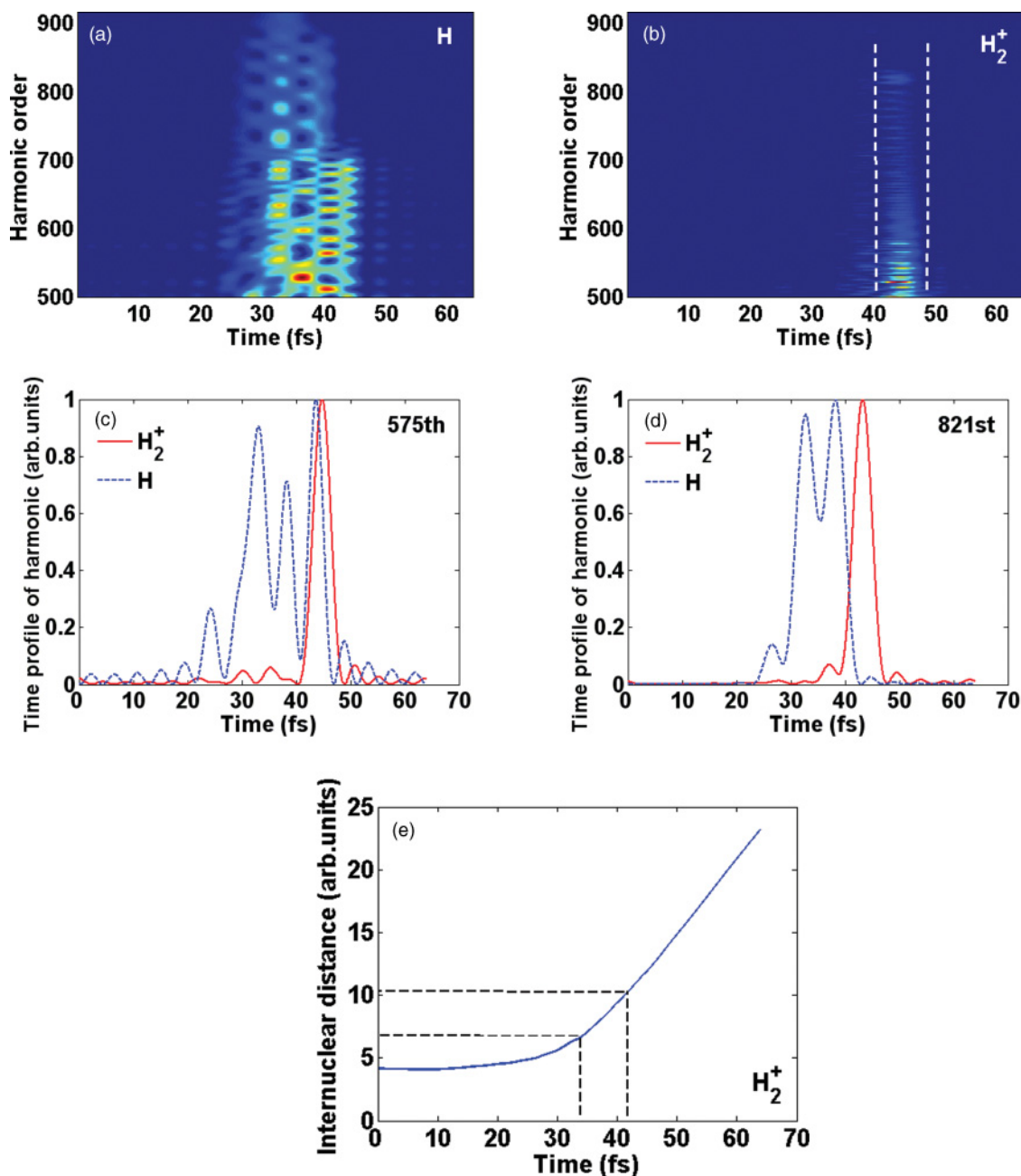


FIG. 3. (Color online) Time profiles of the harmonic spectra from 499th to 915th for the H atom (a) and for the H₂⁺ molecule (b). (c),(d) Time profiles of harmonics (575th and 821st) by performing an inverse Fourier transform for the H₂⁺ molecule (red solid) and for the H atom (blue dashed). (e) Time-dependent internuclear distance for the H₂⁺ molecule.

The isolated attosecond generation is attributed to the CREI and the nuclear motion just as shown in the following text. The time profiles of the harmonic spectra from 499th to 915th are presented in Figs. 3(a) and 3(b). It is interesting to note that for the H₂⁺ molecule the harmonic generation is restricted in the region of 40.3–48.9 fs marked by the dashed line. That is to say that only the pulse appearing in the region of 40.3–48.9 fs is selected for generation with all the other pulses suppressed in the pulse train. Whereas, for the H atom, the harmonic emissions are generated every half-cycle resulting in the creation of attosecond pulse trains. Figures 3(c) and 3(d) represent the time profiles of harmonics (575th and 821st) by

performing an inverse Fourier transform for the H₂⁺ molecule (red solid curve) and for the H atom (blue dashed curve). The red solid and the blue dashed curves in Figs. 3(c) and 3(d) are normalized, respectively. It can be seen more directly that an isolated attosecond pulse is generated from one order of harmonic for the H₂⁺ molecule, while attosecond pulse trains are obtained for the H atom. Therefore when selecting the range of harmonic spectra properly, an isolated attosecond pulse can be produced for the H₂⁺ molecule as shown in Fig. 2. The harmonic emission process can be well explained by a three-step model: Active electrons first tunnel through the potential barrier, are accelerated by laser fields, and then

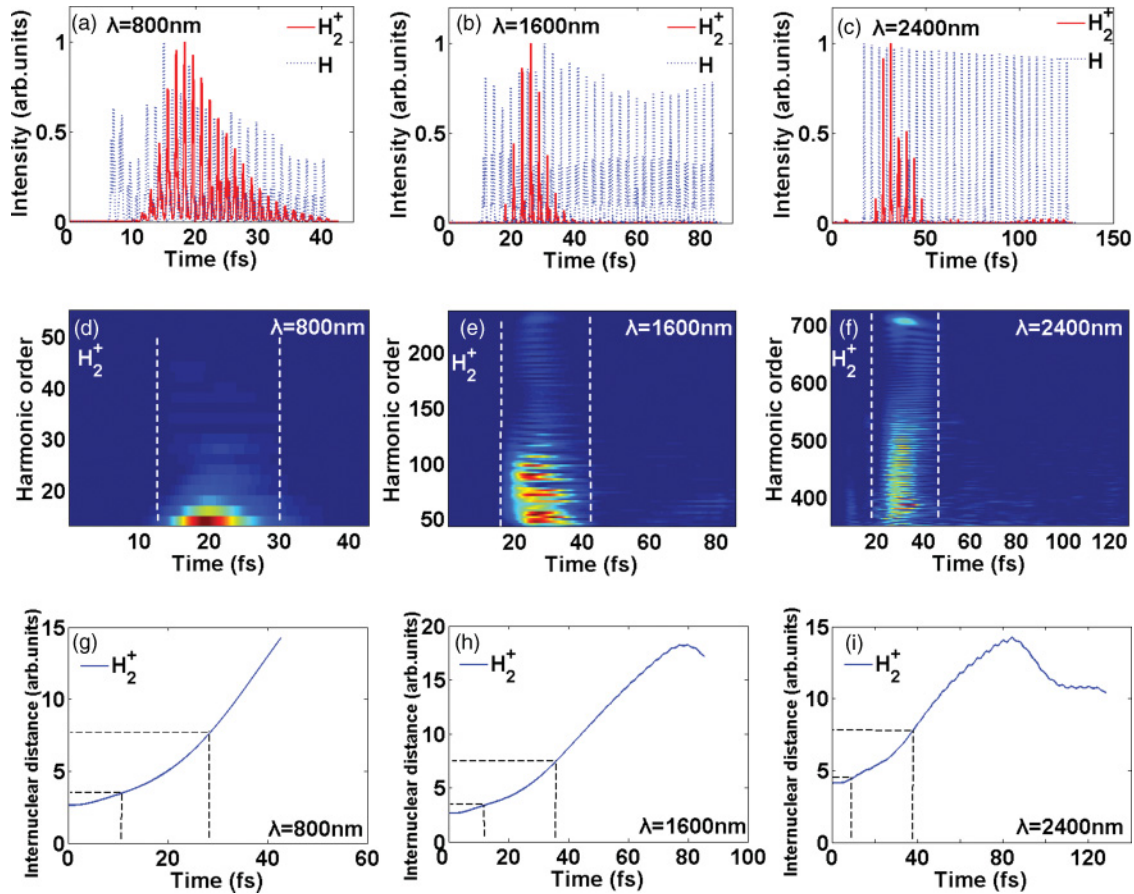


FIG. 4. (Color online) Temporal profiles of the harmonic emission at the cutoff for the H_2^+ molecule (red solid curve) and for the H atom (blue dotted curve), respectively, driven by laser pulse with (a) $\lambda = 800$ nm, (b) $\lambda = 1600$ nm, and (c) $\lambda = 2400$ nm. Diagrams of the time profiles of harmonic spectra for the H_2^+ molecule driven by the laser pulse with (d) $\lambda = 800$ nm, (e) $\lambda = 1600$ nm, and (f) $\lambda = 2400$ nm. Time-dependent internuclear distance for the H_2^+ molecule driven by laser pulse with (g) $\lambda = 800$ nm, (h) $\lambda = 1600$ nm, and (i) $\lambda = 2400$ nm.

recombine with parent ions to emit high-energy photons [31]. Furthermore, the electrons are ionized at about half of an optical cycle earlier than the crest of the electric oscillation adjacent to the moment when the harmonic emission occurs. For the H_2^+ molecule the harmonic emission is confined in the time range from 40.3 to 48.9 fs as shown in Fig. 3(b). This means that the electrons are ionized in the time range from 34.0 to 41.9 fs. At this very moment, the internuclear distance ranges from 6.7 to 10.3 a.u., as shown in Fig. 3(e). As is well known, when R increases to intermediate-to-large internuclear separations ($5 < R < 12$ a.u.), CREI in the H_2^+ molecule is remarkable [16,19]. While for the H atom, the attosecond pulses are generated every half-cycle resulting in the creation of attosecond pulse trains, as shown in Fig. 3(a). For the H_2^+ molecule the nuclear motion is taken into account, which is the only difference between the H_2^+ molecule and the H atom in our model. Thus we think that the CREI and nuclear motion operate in concert resulting in the generation of single attosecond pulses for the H_2^+ molecule. Our scheme suggests that isolated attosecond pulses in two spectral regions—258–323 eV which is well within the water window and 626–691 eV which is beyond the water window—can be produced attributed to the enhanced ionization and concomitant nuclear motion of H_2^+ molecule driven by a 2400-nm, 4×10^{14} W/cm² laser field with a duration of about four optical cycles.

In order to clarify the role of the molecule motion played in the process of isolated attosecond pulse generation and to reduce the influence of the driving laser field as much as possible, we employ an envelope function $f(t)$ that rises during the first half of an optical cycle, decreases during the last half of an optical cycle, and holds constant for the middle fifteen optical cycles. The intensity of the laser pulses is 2×10^{14} W/cm². Figures 4(a), 4(b), and 4(c) show the temporal profiles of the harmonic emission at the cutoff with a bandwidth of ~ 30 eV for the H_2^+ molecule (red solid curve) and for the H atom (blue dotted curve), respectively. Figures 4(d), 4(e), and 4(f) present the time profiles of harmonics for the H_2^+ molecule by performing an inverse Fourier transform of each harmonic from 13th to 55th [Fig. 4(d)], from 43th to 237th [Fig. 4(e)], and from 351st to 725th [Fig. 4(f)]. Figures 4(g), 4(h), and 4(i) illustrate the time-dependent internuclear distance for the H_2^+ molecule. The central wavelengths of the driving laser pulses are 800 nm [Figs. 4(a), 4(d), 4(g)], 1600 nm [Figs. 4(b), 4(e), 4(h)] and 2400 nm [Figs. 4(c), 4(f), 4(i)], respectively. One can see from these figures that the wavelength effect on the selecting of the generation of single attosecond pulses is obvious. The generated attosecond pulse train is shorter for the longer wavelength. This can be understood as that in the long-wavelength laser field, the ponderomotive energies of the nuclei are so large that the nuclei can be efficiently

accelerated and the electron-nuclear motion is prominent. The relevant internuclear distances when the attosecond pulses are generated are from 3.5 to 7.7 a.u. in Fig. 4(g), from 3.4 to 7.5 a.u. in Fig. 4(h), and from 4.5 to 7.8 a.u. in Fig. 4(i). The regions of the internuclear distance in which the attosecond pulses are selected to generate are the same for the different wavelengths. All these prove that the CREI and nuclear motion give rise to the generation of single attosecond pulses.

IV. CONCLUSION

In this work, we propose a scheme to generate isolated attosecond pulses not only in the plateau region (258–323 eV, within the water window) but also at the cutoff (626–691 eV,

beyond the water window) using a multicycle 2400-nm midinfrared laser field with moderate intensity interacting with H_2^+ molecules. The CREI and nuclear motion operate in concert resulting in the generation of single attosecond pulses. Thus, the single attosecond pulse generation provides insight into the nuclear dynamics.

ACKNOWLEDGMENTS

This work is supported by the National Natural Science Foundation (Grants No. 10734080, No. 60921004, No. 11134010, No. 10904157, and No. 61078022), 973Project (Grant No. 2011CB808103), and Shanghai Commission of Science and Technology (Grant No. 10QA1407600).

-
- [1] Z. Chang, A. Rundquist, H. Wang, M. M. Murnane, and H. C. Kapteyn, *Phys. Rev. Lett.* **79**, 2967 (1997).
- [2] E. J. Takahashi, T. Kanai, K. L. Ishikawa, Y. Nabekawa, and K. Midorikawa, *Phys. Rev. Lett.* **101**, 253901 (2008).
- [3] G. Sansone, E. Benedetti, F. Calegari, C. Vozzi, L. Avaldi, R. Flammini, L. Poletto, P. Villoresi, C. Altucci, R. Velotta, S. Stagira, S. De Silvestri, and M. Nisoli, *Science* **314**, 443 (2006).
- [4] M. Drescher, M. Hentschel, R. Kienberger, M. Uiberacker, V. Yakovlev, A. Scrinzi, Th. Westerwalbesloh, U. Kleineberg, U. Heinzmann, and F. Krausz, *Nature* **419**, 803 (2002).
- [5] E. Goulielmakis, M. Schultze, M. Hofstetter, V. S. Yakovlev, J. Gagnon, M. Uiberacker, A. L. Aquila, E. M. Gullikson, D. T. Attwood, R. Kienberger, F. Krausz, and U. Kleineberg, *Science* **320**, 1614 (2008).
- [6] Ch. Spielmann, N. H. Burnett, S. Sartania, R. Koppitsch, M. Schnürer, C. Kan, M. Lenzner, P. Wobrauschek, and F. Krausz, *Science* **278**, 661 (1997).
- [7] X. Gu, G. Marcus, Y. Deng, T. Metzger, C. Teisset, N. Ishii, T. Fuji, A. Baltuška, R. Butkus, V. Pervak, H. Ishizuki, T. Taira, T. Kobayashi, R. Kienberger, and F. Krausz, *Opt. Express* **17**, 62 (2009).
- [8] G. Andriukaitis, T. Balčiūnas, S. Ališauskas, A. Pugžlys, A. Baltuška, T. Popmintchev, M.-C. Chen, M. M. Murnane, and H. C. Kapteyn, *Opt. Lett.* **36**, 2755 (2011).
- [9] C. P. Hauri, R. B. Lopez-Martens, C. I. Blaga, K. D. Schultz, J. Cryan, R. Chirila, P. Colosimo, G. Doumy, A. M. March, C. Roedig, E. Sistrunk, J. Tate, J. Wheeler, L. F. DiMauro, and E. P. Power, *Opt. Lett.* **32**, 868 (2007).
- [10] C. Li, D. Wang, L. Song, J. Liu, P. Liu, C. Xu, Y. Leng, R. Li, and Z. Xu, *Opt. Express* **19**, 6783 (2011).
- [11] M.-C. Chen, P. Arpin, T. Popmintchev, M. Gerrity, B. Zhang, M. Seaberg, D. Popmintchev, M. M. Murnane, and H. C. Kapteyn, *Phys. Rev. Lett.* **105**, 173901 (2010).
- [12] P. Zou, R. Li, Z. Zeng, H. Xiong, P. Liu, Y. Leng, P. Fan, and Z. Xu, *Chin. Phys. B* **19**, 019501 (2010).
- [13] W. Hong, P. Wei, Q. Zhang, S. Wang, and P. Lu, *Opt. Express* **18**, 11308 (2010).
- [14] H. Du and B. Hu, *Opt. Express* **18**, 25958 (2010).
- [15] H. Mashiko, S. Gilbertson, M. Chini, X. Feng, C. Yun, H. Wang, S. D. Khan, S. Chen, and Z. Chang, *Opt. Lett.* **34**, 3337 (2009).
- [16] T. Zuo and A. D. Bandrauk, *Phys. Rev. A* **52**, R2511 (1995).
- [17] T. Seideman, M. Y. Ivanov, and P. B. Corkum, *Phys. Rev. Lett.* **75**, 2819 (1995).
- [18] P. H. Bucksbaum, A. Zavriyev, H. G. Muller, and D. W. Schumacher, *Phys. Rev. Lett.* **64**, 1883 (1990).
- [19] A. D. Bandrauk, S. Chelkowski, S. Kawai, and H. Lu, *Phys. Rev. Lett.* **101**, 153901 (2008).
- [20] S. Baker, J. S. Robinson, C. A. Haworth, H. Teng, R. A. Smith, C. C. Chirilă, M. Lein, J. W. G. Tisch, and J. P. Marangos, *Science* **312**, 424 (2006).
- [21] T. Bredtmann, S. Chelkowski, and A. D. Bandrauk, *Phys. Rev. A* **84**, 021401 (2011).
- [22] A. D. Bandrauk, S. Chelkowski, and I. Kawata, *Phys. Rev. A* **67**, 013407 (2003).
- [23] D. G. Lappas and J. P. Marangos, *J. Phys. B* **33**, 4679 (2000).
- [24] R. Velotta, N. Hay, M. B. Mason, M. Castillejo, and J. P. Marangos, *Phys. Rev. Lett.* **87**, 183901 (2001).
- [25] J. Itatani, D. Zeidler, J. Levesque, M. Spanner, D. M. Villeneuve, and P. B. Corkum, *Phys. Rev. Lett.* **94**, 123902 (2005).
- [26] T. Kreibich, M. Lein, V. Engel, and E. K. U. Gross, *Phys. Rev. Lett.* **87**, 103901 (2001).
- [27] M. Lein, T. Kreibich, E. K. U. Gross, and V. Engel, *Phys. Rev. A* **65**, 033403 (2002).
- [28] M. R. Hermann and J. A. Fleck Jr., *Phys. Rev. A* **38**, 6000 (1988).
- [29] D. Bauer and P. Koval, *Comput. Phys. Commun.* **174**, 396 (2006).
- [30] H. Yu and A. D. Bandrauk, *Phys. Rev. A* **56**, 685 (1997).
- [31] P. B. Corkum, *Phys. Rev. Lett.* **71**, 1994 (1993).